Hindawi
Mathematical Problems in Engineering
Volume 2021, Article ID 6229498, 19 pages
https://doi.org/10.1155/2021/6229498

Research Article

Structural Resistance of Simplified Side Hull Models Accounting for Stiffener Design and Loading Type

Aditya Rio Prabowo,[1] **Tuswan Tuswan**,[2] **Arifin Nurcholis**,[1] **and Anandito Adam Pratama**[1]

[1]*Department of Mechanical Engineering, Universitas Sebelas Maret, Surakarta, Indonesia*
[2]*Department of Naval Architecture, Institut Teknologi Sepuluh Nopember, Surabaya, Indonesia*

Correspondence should be addressed to Aditya Rio Prabowo; aditya@ft.uns.ac.id

Received 11 May 2021; Revised 18 July 2021; Accepted 23 September 2021; Published 4 October 2021

Academic Editor: Suzanne M. Shontz

Thin-walled stiffened panels are fundamental structural components that form the primary structure of the ship hull. The effectiveness of the stiffener configuration design needs to be assessed because members are unavoidably subjected to various load types during operations. In this situation, assessment is required to quantify the responses and determine the relationship between the structural resistance and input parameters. The aim of this work was to obtain structural resistance data on the stiffened side hull of a medium-sized tanker with various model configurations by using finite element analysis with different loading parameters, i.e., load type and angle, as the main inputs. The results indicate that stiffener configurations subjected to loads at the center and random positions influence the effectiveness in reducing the deformation. The results show that the stiffener is more effective when the location of the force is very close to the stiffener. Therefore, higher strength can be obtained with a design in which the area that is not supported by the stiffener is minimized.

1. Introduction

The application of thin-walled steel structures in ships and offshore construction fields has gained popularity in recent decades. The primary designs of ship structures are usually assemblies of plates/shells and stiffeners that are attached in the longitudinal or transverse direction and equally spaced over the plates to provide sufficient strength and stiffness to carry in-plane and out-of-plane loads. The main benefit of reinforcing a plate with stiffeners lies in the tremendous increase in the strength and stability of the structure with a minimum increase in the overall weight. Therefore, to reach the goals of structural and cost efficiency, it is vital to initially assess the structural stability of stiffened panels in the ship structural design phase [1], which is a complex task, because it includes a variety of aspects, including geometry configuration, physical materials, load combination.

The ultimate strength of stiffened plates has been researched from various perspectives by employing different approaches that aim to investigate the influence of combinations of parameters on structural responses. For instance, Paik et al. [2, 3] conducted some benchmark studies on the strength assessment of the bottom part of an AFRAMAX-class oil tanker under combined biaxial compression and lateral pressure. Several factors, including the load types and dimensions, were further analyzed. In 2013, numerical investigations were conducted by Xu et al. [4] to examine the influence of boundary conditions and geometry on the ultimate strength of rectangular stiffened plates of bulk carriers under combined loads. Strength assessment under combined load actions, i.e., longitudinal and lateral loads in stiffened panels, was performed both numerically and experimentally in detail by Shanmugam et al. [5]. Their results indicate that lateral load-carrying capacity drops with an increase in axial load and vice versa. Experimental and numerical investigations on the ultimate strength of stiffened plates subjected to combined biaxial compression and lateral loads showed that lateral pressure enhanced the load-carrying capacity when the lateral force restrained deformation, as investigated by Ma et al. [6]. Further, the ultimate

and residual strength of a hull girder based on IACS CSR-H,CSR-OT, and CSR-BC were compared in detail by Shi et al. [7]. In a series of recent studies, more advanced analyses of stiffened ship structures subjected to impact phenomena were performed to identify structural damage caused by striking and stranding, including ship–ship collision accidents [8–12], ship grounding [13–17], and other forms of ship hull damage [18–22].

For many years, investigating the influence of the stiffener type and configuration on strength behavior has been a topic of interest. A novel Y-stiffener profile for the ship structure was analyzed by Leheta et al. [23] to assess the ultimate strength of the proposed design using IACSCSR for a double-hull oil tanker. Using a similar scenario, the influence of using novel Y-stiffeners on the load-carrying capacity of ship deck panels under the vertical hull-girder bending moment was further studied numerically by Leheta et al. [24]. By conducting a series of experimental tests, Gordo and Soares [25–27] compared U stiffeners with a new shape with panels reinforced by stiffeners with typical shapes to use in high-speed ships. The effect of stiffener geometry on the ultimate strength of the stiffened panels under compression was analyzed. Further, the effects of various configurations of the stiffener cross section were numerically investigated by Ren et al. [28] to determine the most suitable type to replace the original steel stiffener in the upper deck of a warship. The configuration of the stiffener/girder cross section has also been investigated in other structural parts of different kinds of ships, such as the side hull [29], car deck [30], stern ramp door [31], unsymmetrical plate girder [32], and hull girder of a very large crude oil carrier (VLCC) [33]. The design that achieves the highest strength-to-weight ratio is identified as the best.

The influence of the structural assessment of stiffened panels of the ship structure under different loading scenarios has been well studied. However, limited studies are available regarding structural evaluations of stiffened panels subjected to a centralized load, especially when the side hull hits something with a sharp tip. To address these issues, additional studies are required to provide deeper insights into the effects of those parameters. In particular, a numerical investigation using finite element analysis is needed to study the mechanical reaction of the side hull of a ship with different stiffener designs under concentrated loads applied to the center of the plate and to random positions. The present study aimed to further investigate the relationship between the behavior of a stiffened side hull with various stiffener configurations and variations in uncertain load types and angles. In this regard, the geometry and cross section of the side hull structure of a medium-sized tanker were used as a reference model. This work describes the finite element results of both contour descriptions and data descriptions.

2. State of the Art

In the ship structure, the force types acting on a stiffened plate are in-plane compression or tension from the overall hull-girder bending moment or torsion, the shear force resulting from the hull-girder shear force, and lateral pressure from the external wave or shock loading [34]. However, the possibility that a ship structure will be damaged by several types of accidents, including striking and stranding with any other objects, is crucial to investigate [35]. In fact, the force that occurs during stranding has an uncertain direction, and it will also cause an uncertain force distribution on the stiffened hull plate. To improve the stiffened plate design, one must determine the structural response to a concentrated load with various force directions. However, it would be challenging to conduct experimental tests using these input parameters. Using finite element analysis, the stiffened plate can be subjected to loads with various force directions and angles simultaneously to determine the structural response. The finite element outputs of von Mises stress, strain, and displacement were used to compare the behavior of all developed models. The von Mises stress is the equivalent or effective stress at which yielding is predicted to occur in ductile materials. To analytically compute von Mises stress, stress is derived using principal axes in terms of principal stresses [36]. The relations between external forces, which characterize stress, and the deformation of the body, which describes strain, are called stress-strain relations. In simple form, Hooke's law for one dimension, or the condition of stress and strain for elastic materials, is given by

$$\sigma = E\varepsilon, \tag{1}$$

where σ is the stress, E is Young's modulus, and ε is the strain.

Then, the strain energy per unit volume for simple tension is expressed as follows:

$$u = \int_0^{\varepsilon} \sigma \, \mathrm{d}\varepsilon = \int_0^{\varepsilon} E\varepsilon \, \mathrm{d}\varepsilon = \frac{1}{2}E\varepsilon^2 = \frac{1}{2}\varepsilon\sigma. \tag{2}$$

For the state of stress, total strain energy per unit volume is defined as

$$u = \frac{1}{2}\left(\varepsilon_1\sigma_1 + \varepsilon_2\sigma_2 + \varepsilon_3\sigma_3\right). \tag{3}$$

Using the principle of superposition, the generalized Hooke's law for a three-dimensional state of stress and strain in a homogeneous and isotropic material can be expressed as a matrix:

$$\begin{bmatrix} \varepsilon_1 \\ \varepsilon_2 \\ \varepsilon_3 \end{bmatrix} = \frac{1}{E}\begin{bmatrix} 1 & -\nu & 0 \\ -\nu & 1 & 0 \\ 0 & 0 & 2(1+\nu) \end{bmatrix}\begin{bmatrix} \sigma_1 \\ \sigma_2 \\ \sigma_3 \end{bmatrix}. \tag{4}$$

This analysis can be readily extended to a triaxial state of stress, expressed as follows:

$$\varepsilon_1 = \frac{1}{E}\left[\sigma_1 - \nu\left(\sigma_2 + \sigma_3\right)\right], \tag{5}$$

$$\varepsilon_2 = \frac{1}{E}\left[\sigma_2 - \nu\left(\sigma_1 + \sigma_3\right)\right], \tag{6}$$

$$\varepsilon_3 = \frac{1}{E}\left[\sigma_3 - \nu(\sigma_1 + \sigma_2)\right], \quad (7)$$

where ν is Poisson's ratio. Further, equations (5)–(7) are substituted into equation (3), so that the equation of total strain energy can be obtained:

$$u = \frac{1}{2E}\left[\sigma_1^2 + \sigma_2^2 + \sigma_3^2 - 2\nu\left(\sigma_1\sigma_2 + \sigma_2\sigma_3 + \sigma_3\sigma_1\right)\right]. \quad (8)$$

By letting $\sigma_1 = \sigma_2 = \sigma_3 = \sigma_{av}$ in equation (8), we obtain the strain energy associated with hydrostatic loading, or only volume change, as follows:

$$u_v = \frac{1-2\nu}{6E}\left[\sigma_1^2 + \sigma_2^2 + \sigma_3^2 + 2\left(\sigma_1\sigma_2 + \sigma_2\sigma_3 + \sigma_3\sigma_1\right)\right]. \quad (9)$$

The distortion energy per unit volume assumes that

$$u_d = u - u_v. \quad (10)$$

Then, distortion energy per unit volume can be written as

$$u_d = \frac{1+\nu}{3E}\left[\frac{\left(\sigma_1 - \sigma_2\right)^2 + \left(\sigma_2 - \sigma_3\right)^2 + \left(\sigma_3 - \sigma_1\right)^2}{2}\right]. \quad (11)$$

As it is assumed that $u_d = 0$ and $\sigma_1 = S_y$, $\sigma_2 = \sigma_3 = 0$, equation (11) can be reduced to

$$u_d = \frac{1+\nu}{3E} S_y^2, \quad (12)$$

where S_y is the yield stress of the material. Yield is predicted to occur if the value of u_d in equation (11) equals or exceeds the value of u_d in equation (12). Furthermore, yield occurs whenever

$$\left[\frac{\left(\sigma_1 - \sigma_2\right)^2 + \left(\sigma_2 - \sigma_3\right)^2 + \left(\sigma_3 - \sigma_1\right)^2}{2}\right]^{1/2} \geq S_y. \quad (13)$$

The left side of equation (13) represents the equivalent or effective stress at which yielding occurs. This stress is usually denoted as σ_v and is known as von Mises stress:

$$\sigma_v = \sqrt{\frac{\left(\sigma_1 - \sigma_2\right) + \left(\sigma_2 - \sigma_3\right) + \left(\sigma_3 - \sigma_1\right)}{2}}. \quad (14)$$

To solve the deformation in the plate, we can use the Kirchhoff assumption. The deformation function is expressed as follows:

$$\kappa_x = -\frac{\partial^2 \omega}{\partial x^2},$$

$$\kappa_y = -\frac{\partial^2 \omega}{\partial y^2}, \quad (15)$$

$$\kappa_{xy} = -\frac{\partial^2 \omega}{\partial x\, \partial y},$$

where K is the curvature in a certain direction or plane; ω is the deflection; and (x, y) is the position in the Cartesian coordinate systems.

The shell element is most well-known for its application in plated structure analysis. Several of the mentioned pioneering works used this element, the intention of which is to perform time-effective calculations. However, the solid element in finite element analysis has certain advantages compared to the shell and has desirable characteristics in numerical calculations: i.e., the solid element has no geometric limitations, requires no geometric preprocessing, and allows stress and strain to be profiled through the thickness. Nevertheless, both the shell and solid elements are equally superior in terms of the meshing freedom. Considering that most of the recommended element size configurations are intended for the shell-implemented structure, an integrated study is necessary to calculate the structure with solid elements. Therefore, the current work aimed to assess the characteristics of idealized structural behavior based on a thin-walled structure, in which the geometrical subject is implemented by solid elements. The current findings were compared with the meshing configuration of shell elements as part of developing reasonable meshing criteria for geometries with solid elements. Subsequently, the acquired criteria were applied to the geometry, which was designated as the subject of finite element calculations.

3. Finite Element Analysis

3.1. Stiffened Side Hull Geometry and Discretization. In the present study, a stiffened, thin-walled ship hull was investigated. The stiffened, thin-walled ship hull consists of a flat plate and flat bar stiffener. The extent and geometrical dimensions of these models were designed based on previous studies [37]. For modeling purposes, in the first step, the geometry of the thin-walled plates was designed. The stiffened plate length and width are 1200 mm and 720 mm, respectively, while the thickness is 5 mm. The flat bar stiffener's dimensions are described by its height and thickness, which are 120 mm and 6 mm. The analysis was performed on four different models that differ in their stiffener configurations, namely, a plate with one stiffener in the longitudinal direction, a plate with two longitudinal stiffeners, a plate with two intersecting stiffeners, and a plate with four symmetrically intersecting stiffeners. Illustrations of the isometric views of the geometrical shapes of the four model configurations are shown in Figures 1 and 2.

The four proposed model configurations use AISI 1045 medium carbon steel, which is taken from Fusion Property Manager, which is comparable to steel manufacturer sheet guides [38–41], for both the plate and the flat bar. In this analysis, the material is assumed to be homogeneous and isotropic with elastic properties. The typical characteristics and physical properties of the proposed materials used for finite element analysis are shown in Table 1.

3.2. Finite Element Model Development. In this investigation, simulations were implemented numerically using a finite element software package. The finite element method is a numerical technique, ideally suited to digital computers, in which a continuous elastic structure (continuum) is discretized into smaller but finite substructures (elements) that can be represented by comprehensive equations [42]. In this

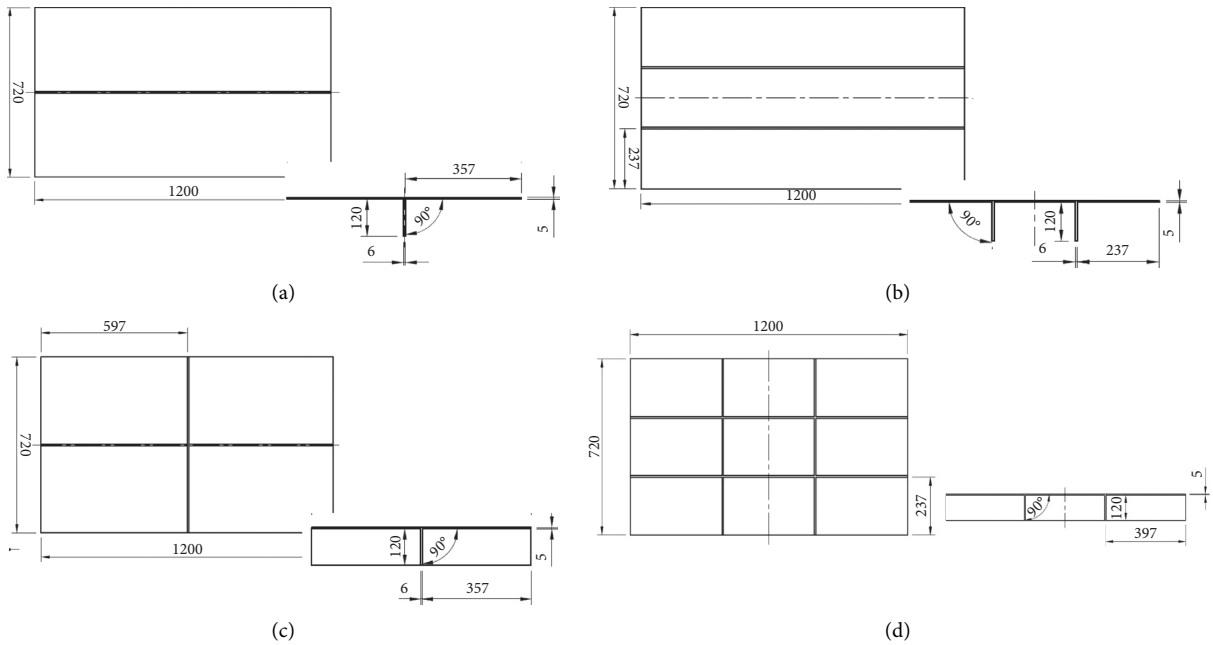

Figure 1: Technical drawing of the stiffened plate models. (a) Plate with one longitudinal stiffener. (b) Plate with two longitudinal stiffeners. (c) Plate with two intersecting stiffeners. (d) Plate with four symmetrically intersecting stiffeners.

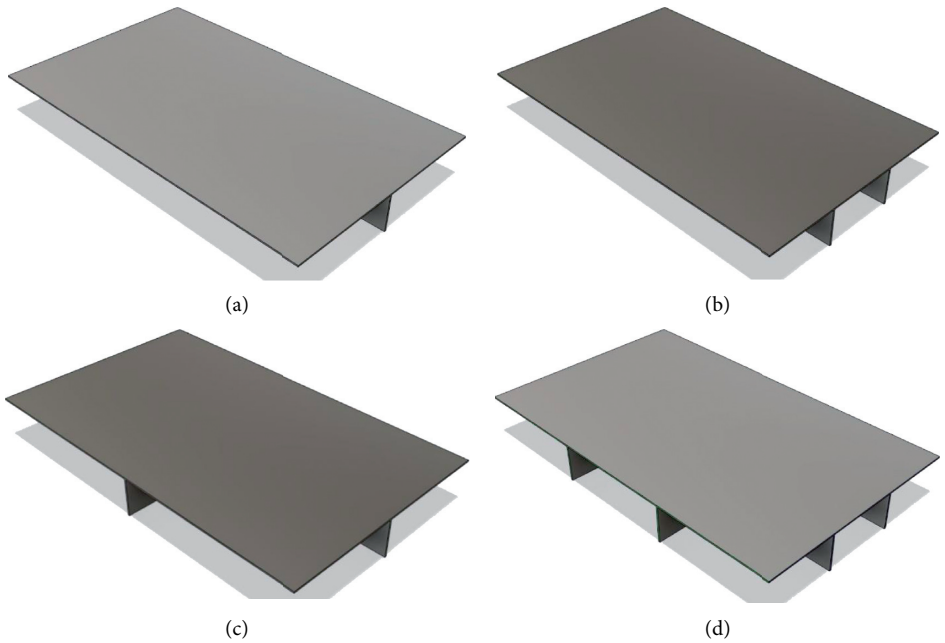

Figure 2: Isometric 3D view of stiffener configuration models. (a) Plate with one longitudinal stiffener. (b) Plate with two longitudinal stiffeners. (c) Plate with two intersecting stiffeners. (d) Plate with four symmetrically intersecting stiffeners.

work, Autodesk Fusion 360 was selected as an FEA tool for modeling and simulation, which can be divided into three steps, as follows:

(1) The 3D model of stiffened hull plate is discretized using Autodesk Fusion 360

(2) The material type, loading scenario, and constraints are applied

(3) Static linear analysis is performed to analyze the physical influence of the mentioned parameters

In the model discretization, the stiffened plate is modeled using solid elements. In this regard, fixed constraints ($U_x = U_y = U_z = 0$) are applied on the four sides of the plate. The plate is subjected to a static concentrated loading force with a magnitude of 5000 N on the z-axis on the upper side of the plate with the assumption that there is no force in other directions (x- and y-axes). The load is applied perpendicular to the upper section of the plate using three loading positions, namely, at the center of the plate and random positions (E2 and E3 positions), as depicted in

Table 1: Material details of the base plate and stiffeners (data are summarized from [38–41]).

Chemical element	Content (%)
Carbon (C)	0.42–0.50
Iron (Fe)	98.51–98.98
Manganese (Mn)	0.60–0.90
Phosphorous (P)	≤0.040
Sulfur (S)	≤0.050
Mechanical property	**Metric**
Density (kg/mm^3)	7.87×10^{-6}
Young's modulus (MPa)	200000
Poisson's ratio	0.29
Yield strength (MPa)	310
Ultimate tensile strength (MPa)	565
Shear modulus (MPa)	80000
Bulk modulus (MPa)	140000
Elongation at break (in 50 mm-%)	16.0
Reduction of area (%)	40.0
Hardness (Brinell)	163
Hardness (Rockwell B)	84

Figure 3. The first load is applied at the center position with respect to the x- and y-axes. The E2 position is located at 618 mm with respect to the x-axis and 599 mm with respect to the y-axis, and the E3 position is located at 139 mm with respect to the x-axis and 162 mm with respect to the y-axis. Besides the variation of the loading position, the model configuration is also varied by applying three loading direction angles with respect to the y-axis, namely, 30°, 60°, and 90°.

A total of 12 main variations were analyzed, starting with the variation of the stiffener configuration and position of the load. Further, for each of the variations, the simulations were then extended by investigating the influence of loading angles. The proposed model scenarios with a total of 36 variations are illustrated in Figure 4 for discrete model and Figure 5 for the scenario list.

4. References for FEA Benchmarking

4.1. Mesh Convergence: Plate with One Longitudinal Stiffener. Convergence assessment was carried out before the main analysis to find the appropriate mesh size for specific geometries with solid elements. The applied mesh size was the main variable that varied between test cases. Previous works by Törnqvist [43], Alsos and Amdahl [44], and Prabowo et al. [45] implemented the element length-to-thickness (ELT) ratio for a plated structure defined with shell elements. In their works, ELT ratios in the range 5–10 were commonly used for finite element analysis, especially for crashworthiness analysis. In this work, structural responses, i.e., stress, displacement, and strain, were quantified to find the most appropriate mesh size, which is represented by the ELT ratio in the final convergence. In the FE setting, the mesh sizes are set to range from 10 to 70 mm. For the first geometry, the simulation was performed for a plate with one longitudinal stiffener, where the load was applied perpendicular to the plate surface. The results of the analysis are presented in Figure 6, which indicates that, for this geometry, the mesh size tends to be stable in the range of 20–50 mm. The convergence data were compiled, and the x-axis values were changed into ELT ratios by dividing the mesh size by the plate thickness, while values on the y-axis were divided by the average value to determine their respective behaviors. The resulting data are displayed in Figure 7, which indicates that ELT ratios in ranges of 4–10 are the best for the plate with one longitudinal stiffener using solid elements. An ELT ratio of 2 is excluded since disparities in the stress and strain are quite high, which almost reach 1.5 or the highest among all displayed tendencies.

4.2. Mesh Convergence: Plate with Two Intersecting Stiffeners. With the same setting, finite element analysis continued for the next geometry, which is the plate with two intersecting stiffeners. Based on the observation of the structural behaviors in Figure 8, the tendency of the results is more stable for mesh sizes ranging from 30 to 70 mm. For 10 and 20 mm, the results display an increasing trend toward a stable state. After this observation, the analysis was focused on verifying the ELT ratio for stress, displacement, and strain. The same treatment as in the analysis of the plate with one stiffener was applied to obtain the recommended ratio. As presented in Figure 9, the displacement ratio is found to be in a stable state for all designated ratios. A similar pattern is also observed in the data assessment of the plate with one longitudinal stiffener. Furthermore, a ratio of 2 is not recommended, as a large distance from the convergence line is observed. However, ratios of 12 and 14 are distinctive, as they are more stable near the convergence line without apparent fluctuations. Based on these results and in consideration of the previous geometry, the recommended ELT ratio to use for the geometry with solid elements ranges from 4 to 10. It is possible to increase the ratio to reduce processing time, but a proper convergence assessment needs to be conducted to ensure that the implemented mesh produces dependable results that fulfill effectiveness (accuracy/fidelity) and efficiency requirements (time calculation) [46].

4.3. Validation Test. For validation purposes, a comparison of the responses between finite element analysis and experimental test was conducted by comparing von Mises stress, displacement, and strain of the plates with one longitudinal stiffener (flat bar) and two longitudinal stiffeners. A previous study [37] has conducted a series of panel penetration tests subjected to grounding load at the center of the plate by a cone shaped indenter at two different stiffened plate models. In this numerical test, the geometrical configuration and test setup referred to the experimental test [37]. The validation test was conducted by comparing the penetration test result illustrated by the force–indentation curves at load 5000 N. Table 2 shows the comparison of von Mises stress, displacement, and strain between present study and previous experimental test. The mean error of numerical result at 3.48% in one stiffener model and 5.75% at two longitudinal stiffeners model indicates good agreement of the proposed finite element modeling. Moreover, the comparison of contour of indentation between experimental

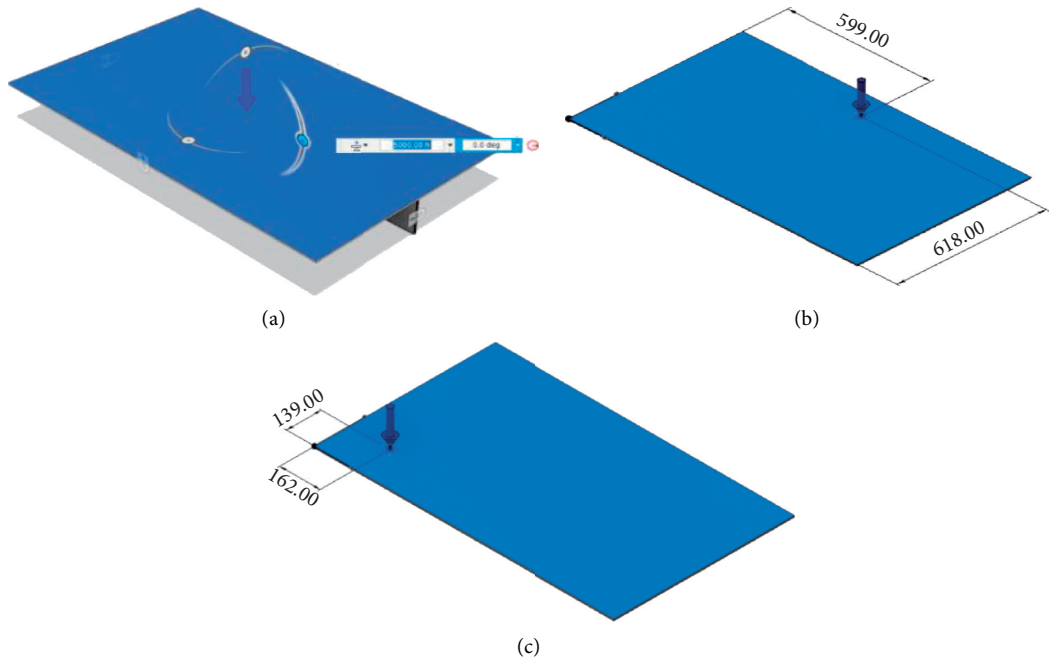

Figure 3: Isometric view of the various loading positions. (a) At center position of plate. (b) At E2 position of plate. (c) At E3 position of plate.

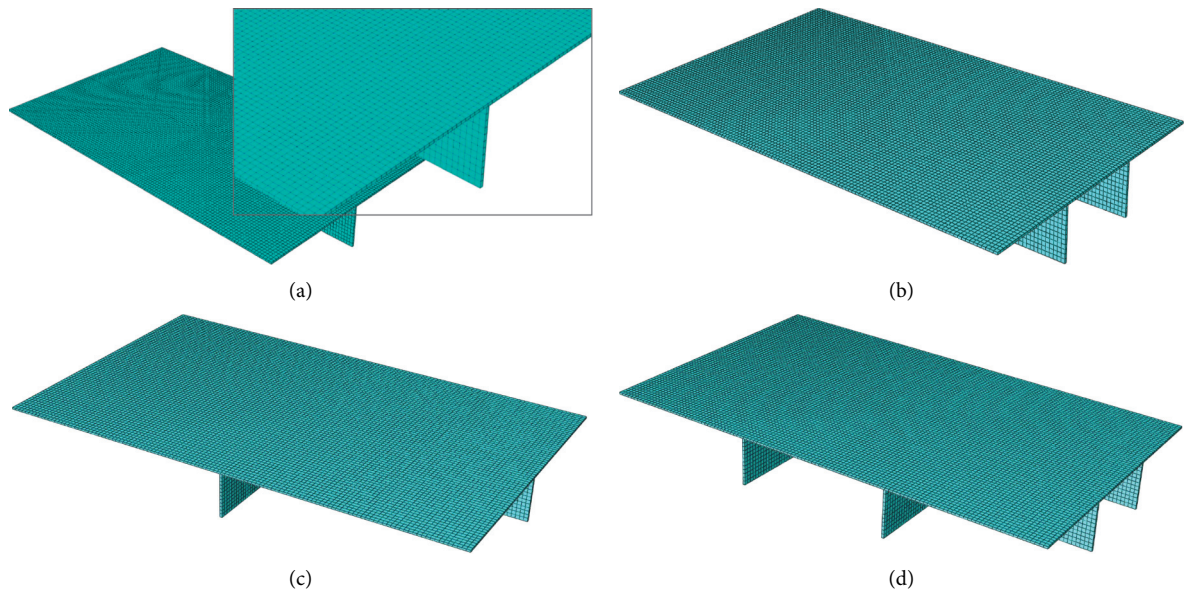

Figure 4: Isometric 3D views of stiffener configuration models: discrete geometry for analysis. (a) Plate with one longitudinal stiffener. (b) Plate with two longitudinal stiffeners. (c) Plate with two intersecting stiffeners. (d) Plate with four symmetrically intersecting stiffeners.

test and numerical test of both stiffened plate models is depicted in Figure 10.

5. Integrated Finite Element Analysis

5.1. Comparison of von Mises Stress Results

5.1.1. Comparison of von Mises Stress for Various Stiffener Configurations. In this section, von Mises stress results for various stiffener configurations are reviewed. Figure 11 compares maximum von Mises stress values for various stiffener configurations with different loading positions. The objective is to compare the behavior of the stiffener design of the stiffened side hull when it hits something with a sharp tip in various locations. All simulation model results in Figures 11(a)–11(11(d)) show that the larger the loading angle, the greater the von Mises stress that occurs. This is because when the force has a small angle, part of the force is distributed horizontally. The result for the stiffened plate with one stiffener (see Figure 11(a)) shows that the design

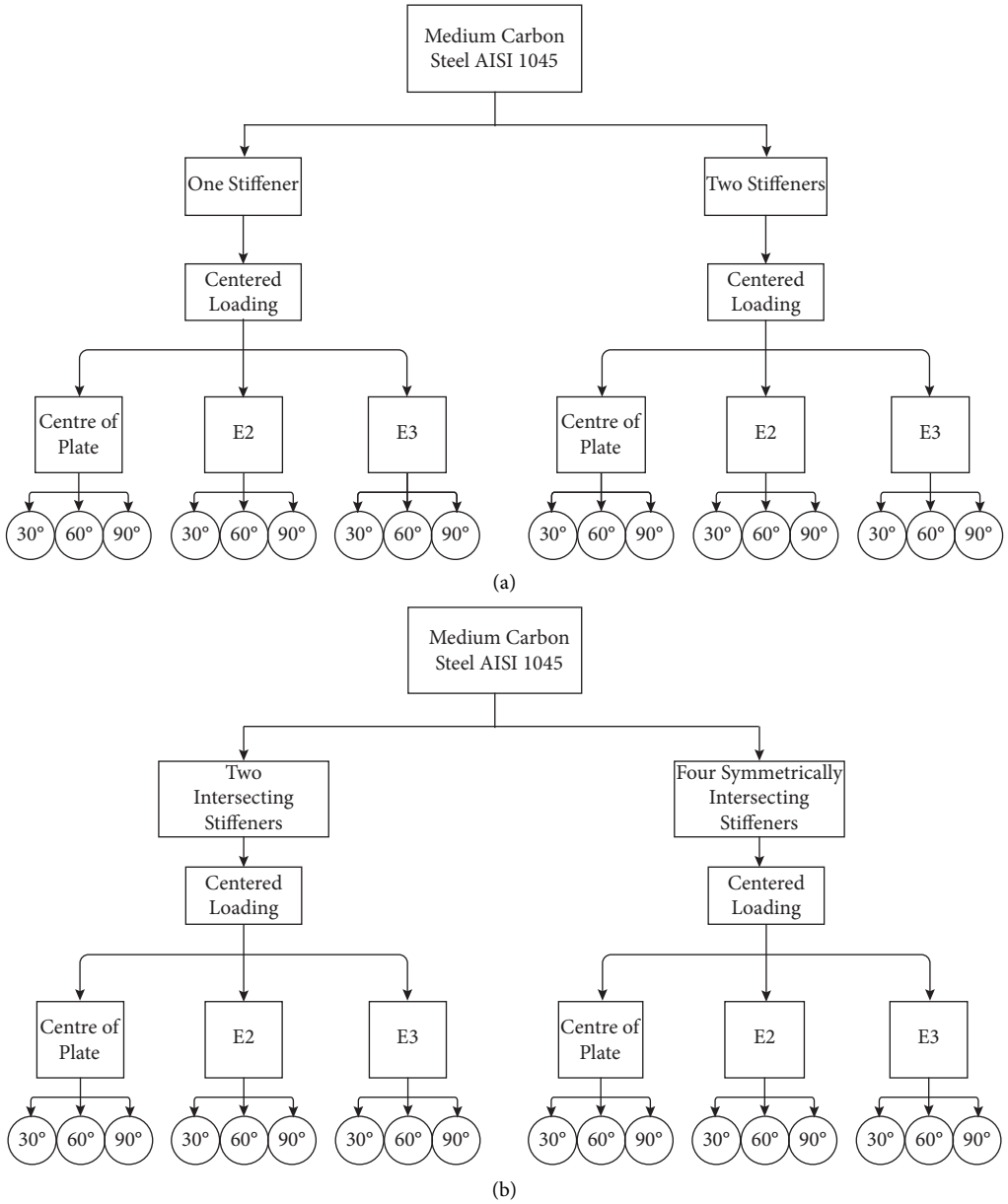

Figure 5: Proposed model scenarios with a total of 36 variations. (a) Model scenarios with one longitudinal stiffener and two longitudinal stiffeners. (b) Model scenarios with two intersecting stiffeners and four symmetrically intersecting stiffeners.

configuration can withstand the load at the center of the object with lower stress than in other load positions. This is because the center of the applied load will be at the center of the stiffener. A similar result is found in Figure 11(c), in which the configuration of two intersecting stiffeners is recommended to withstand loads applied at the center and E2 position. The load applied at the E3 position experiences higher stress, because a large area is not supported by a stiffener. The stiffener configuration is found to be more effective when the applied load is very close to the stiffener. This phenomenon is highlighted in detail in Figures 11(b) and 11(d). In the model with two stiffeners, the lowest stress occurs where the central load is applied, because it is closest to the stiffener. In contrast, the load at the E2 position, which is farthest from the stiffener, encounters the highest stress. Further, the stress in the stiffened plate with four symmetrically intersecting stiffeners can withstand the load at the E2 position, but the applied loads at the E3 position and center experience higher stress.

5.1.2. Comparison of von Mises Stress for Different Stiffener Configurations. To obtain the best model configuration at certain load positions, a comparison of von Mises stress for various stiffener configurations at each load position needs to be plotted. Figure 12(a) illustrates the comparison of stress for different stiffener configurations when the load is applied at the center. The models with one stiffener and two intersecting stiffeners are found to be the best configurations when subjected to a concentrated load at the center position

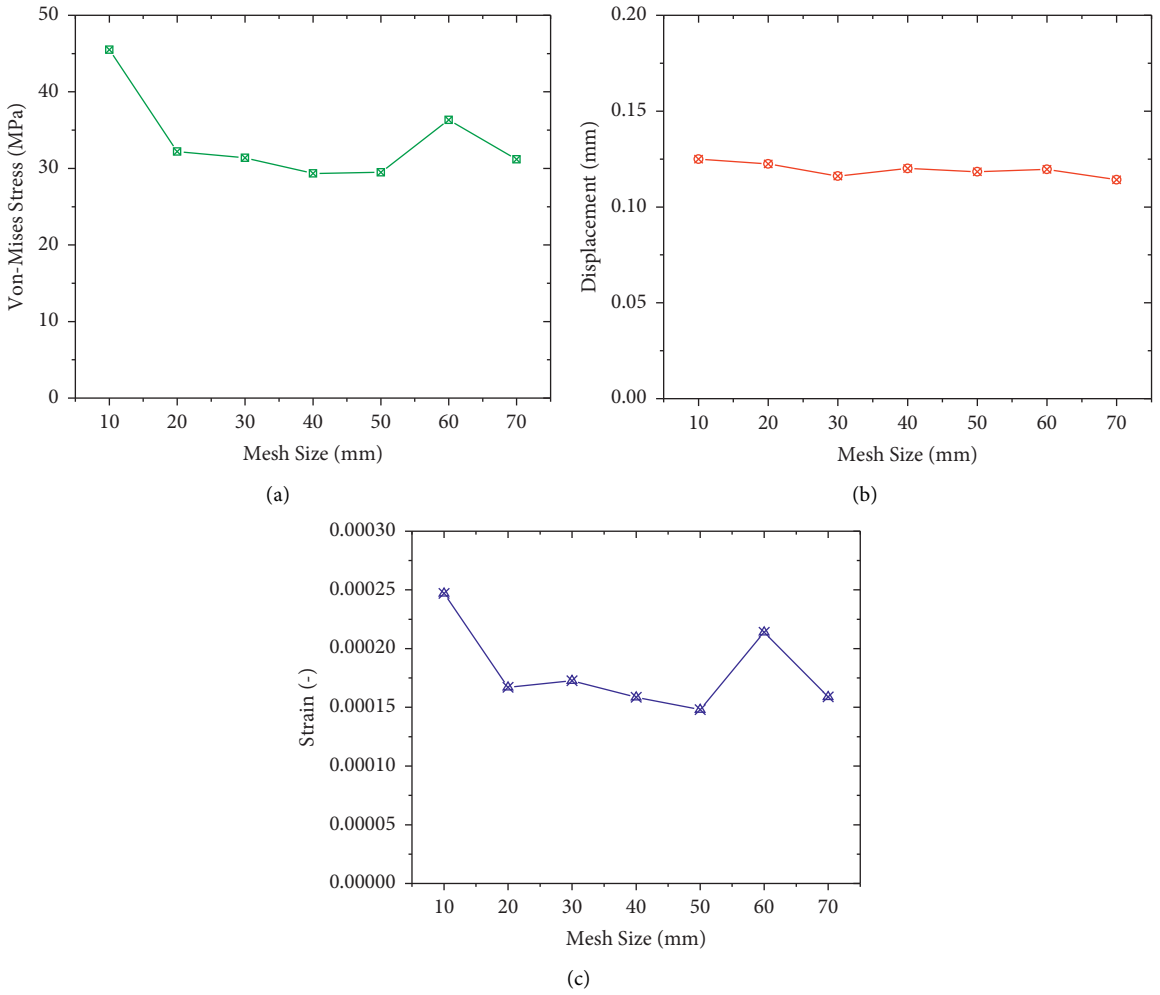

Figure 6: Behaviors of the plate with one longitudinal stiffener subjected to mesh size variation. (a) von Mises stress. (b) Displacement. (c) Strain.

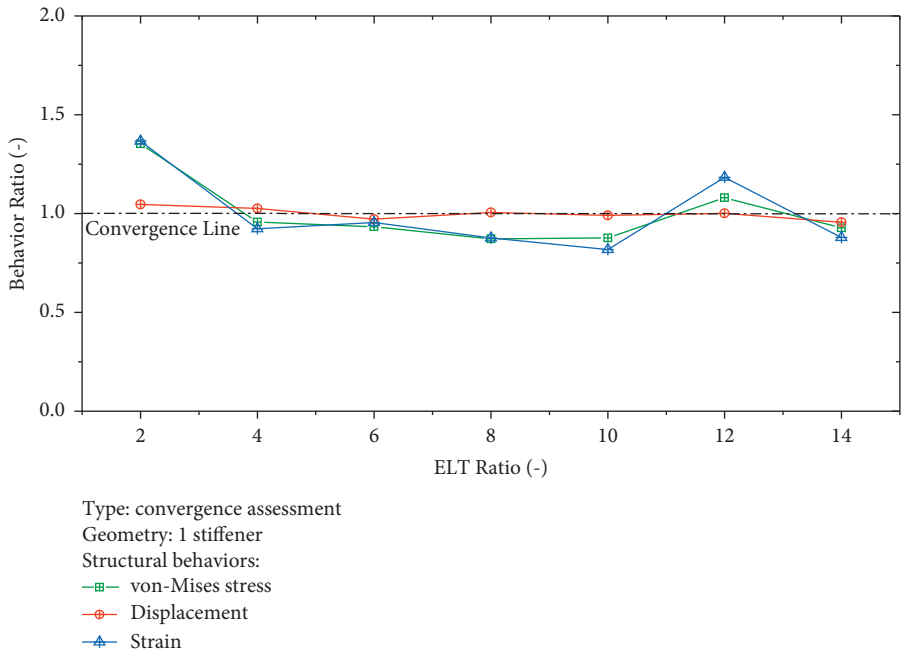

Figure 7: Summary of the convergence assessment of the plate with one longitudinal stiffener.

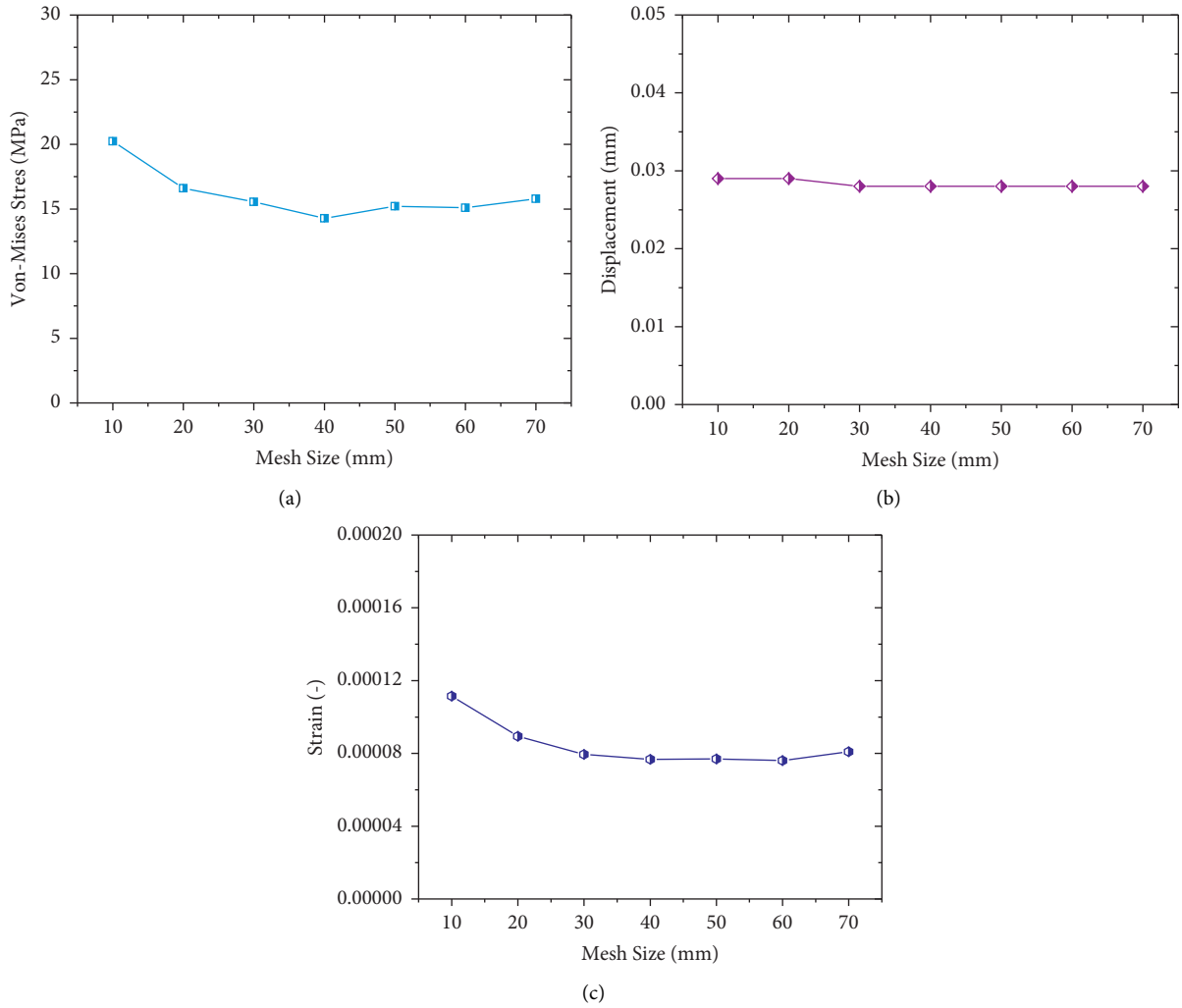

Figure 8: Behaviors of the plate with two intersecting stiffeners subjected to mesh size variation. (a) von Mises stress. (b) Displacement. (c) Strain.

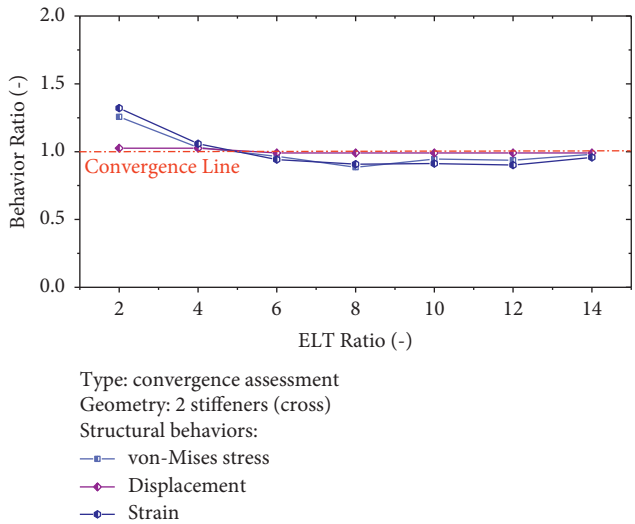

Figure 9: Summary of the convergence assessment on the plate with two intersecting stiffeners.

of the plate. This happens because the location of the load at the center point is really in the middle of the stiffener, so the design configuration is more rigid when exposed to this load. On the other hand, for the stress behavior of the models subjected to random loads (at E2 and E3 positions), the model configurations with two stiffeners and four symmetrically intersecting stiffeners are the best options, as observed in Figures 12(b) and 12(c).

5.2. Comparison of Displacement Values

5.2.1. Comparison of Displacement Values for Various Stiffener Configurations. In this section, the maximum displacement value is used to determine the displacement pattern in different scenarios of the applied load. The resulting effect on the displacement values in all evaluated models is similar to the phenomenon that occurred in the stress results in the previous section. The comparison of deformation results for various stiffener configurations with different loading positions and angles is summarized in Figure 13. As can be seen, the

Table 2: Validation test between finite element analysis and laboratory experiment.

	von Mises stress (MPa)		Error (%)
	FEM (present study)	Experimental test [37]	
Plate with one longitudinal stiffener	27.2	26.56	3.61
Plate with two longitudinal stiffeners	169.4	179.6	5.67
	Displacement (mm)		Error (%)
	FEM (present study)	Experimental test [37]	
Plate with one longitudinal stiffener	0.138	0.135	2.22
Plate with two longitudinal stiffeners	0.854	0.913	6.46
	Strain (—)		Error (%)
	FEM (present study)	Experimental test [37]	
Plate with one longitudinal stiffener	0.000136	0.00013	4.61
Plate with two longitudinal stiffeners	0.000854	0.00090	5.11

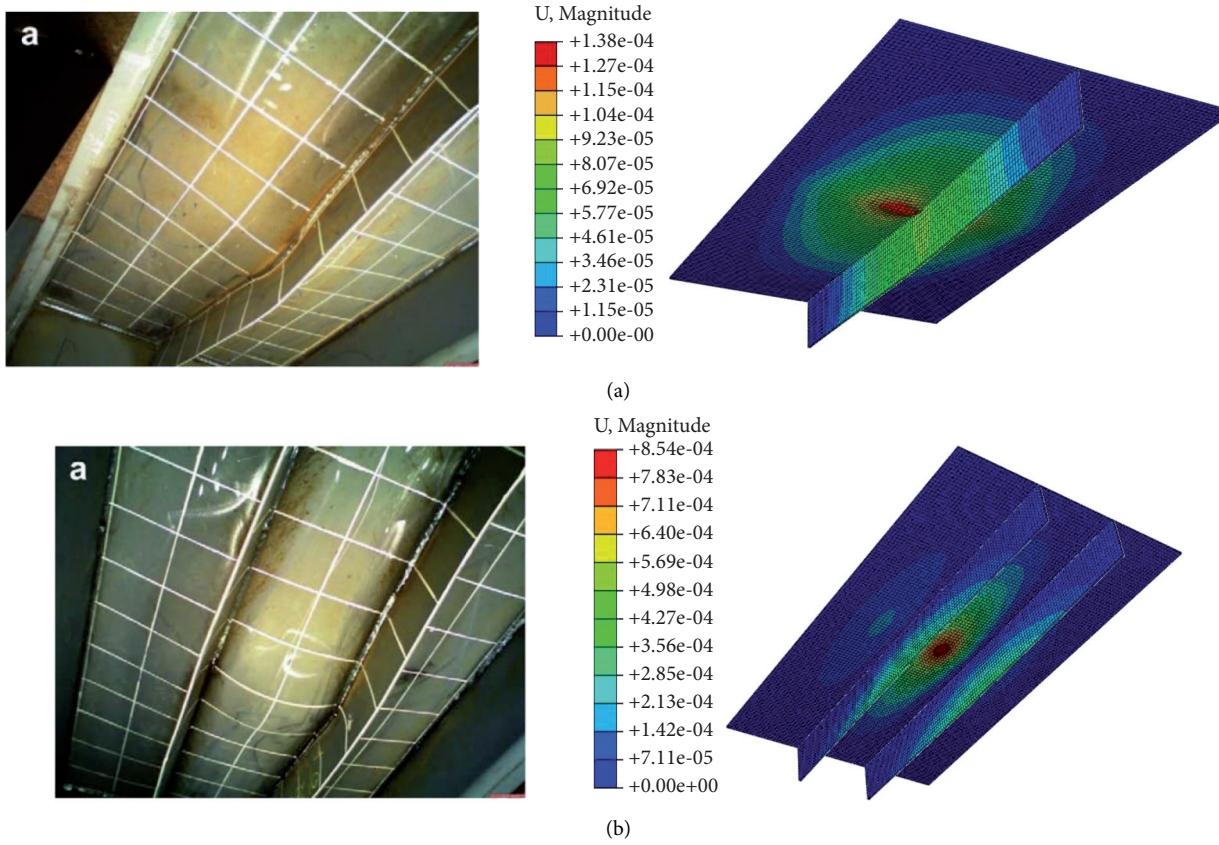

Figure 10: Comparison of deformation contour between experimental test [37] and numerical test. (a) One longitudinal stiffener. (b) Two longitudinal stiffeners.

deformation value increases as the loading angle increases for all evaluated model configurations. The force received by the plate increases, because the force tends to be fully distributed over the plate. As shown in Figure 13(a), the configuration with one stiffener experiences the lowest deformation when the model is subjected to a load at the center position. In contrast, the highest deformation is found for the load applied at the E3 position. This occurs because the largest area of the plate is not reinforced by the stiffener, so more significant deformation occurs. The model configuration with two stiffeners results in the lowest deformation in response to the load at the E3 position. The deformation is the most significant when the load is at the center of the plate. This can occur when the area that is not supported by a stiffener is large. Further, the deformation results for the model with two intersecting stiffeners can be found in Figure 13(c). It can be observed that the model with two intersecting stiffeners is the superior configuration for withstanding a load applied at the center point of the plate and the E2 position. The results indicate that the design is more rigid when subjected to a load that is really in the middle of the stiffener. Moreover, the deformation in the model with four symmetrically intersecting stiffeners subjected to a load at a

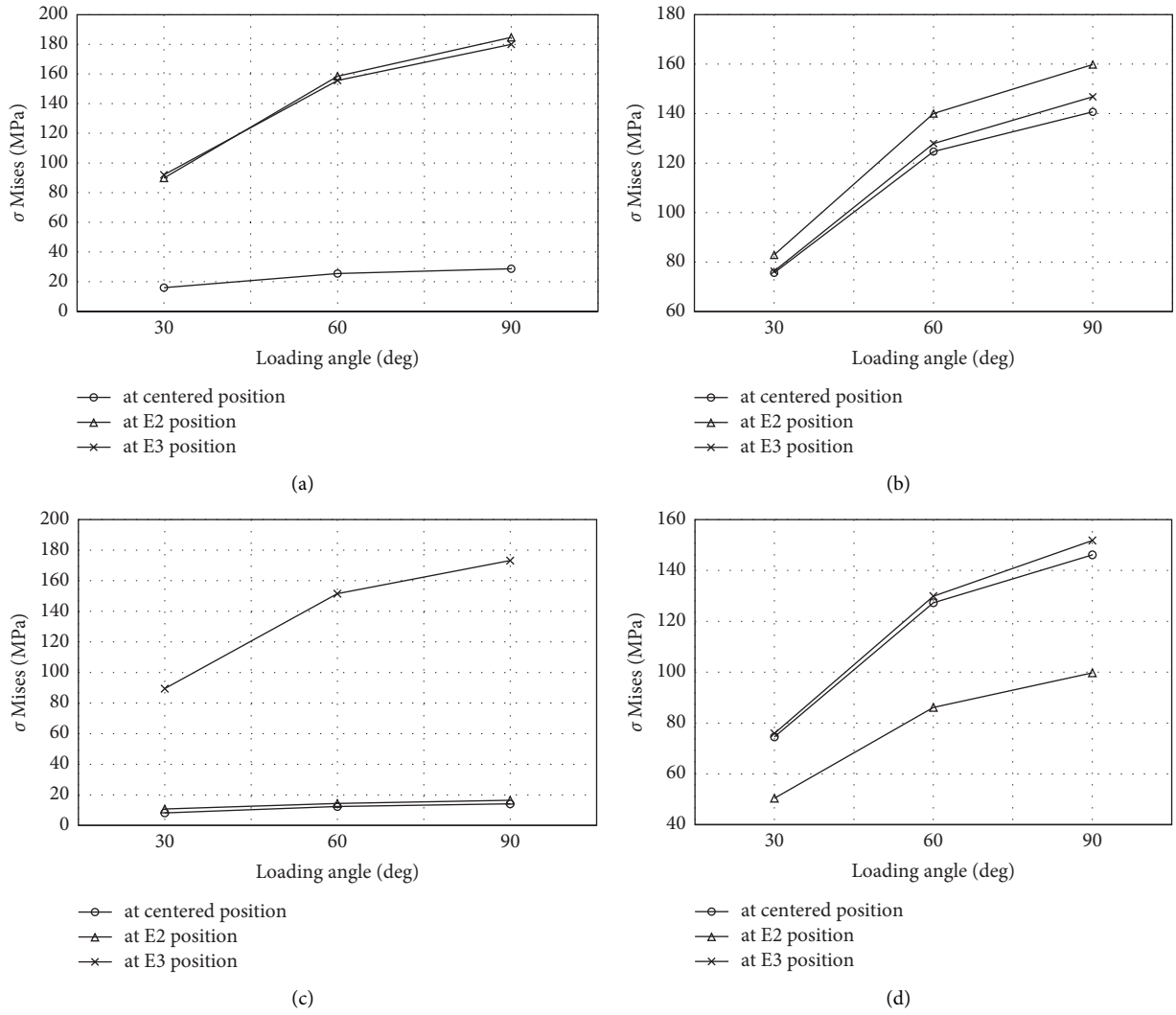

Figure 11: von Mises stress results with various stiffener configurations. (a) One stiffener. (b) Two stiffeners. (c) Two intersecting stiffeners. (d) Four symmetrically intersecting stiffeners.

position near the stiffener is illustrated in Figure 13(d). The results indicate that the smaller the total area that is not supported by the stiffener, the lower the deformation. It can be observed that the model has lower deformation in the E2 position than the other loading positions, whereas deformation values resulting from the load at the center point and E3 position are similar.

5.2.2. Comparison of Displacement at Different Loading Positions. To select the best stiffener model configuration at each load position, a comparison of the deformation at each load position is plotted in Figure 14. The results show that the model with the configuration of two intersecting stiffeners is the best design when it is subjected to a load at the center of the plate. A similar result is found in Figure 14(b), where the model with two intersecting stiffeners is the best option when it is subjected to a concentrated load at the E2 position. Further, the best model configuration with a load at the E3 point can be chosen from the models with two stiffeners and four symmetrically intersecting stiffeners, which have similar displacement values.

5.3. Comparison of Equivalent Strain

5.3.1. Comparison of Equivalent Strain for Various Stiffener Configurations. In this work, a scalar quantity named the equivalent strain is used to describe the state of strain. Figure 15 shows the equivalent strain results from the numerical simulation of all proposed models. According to these results, the strain value increases as the direction of the loading angle increases in all evaluated models. As shown in Figure 15(a), the model with one stiffener results in the lowest strain when subjected to a load at the center position. Conversely, the highest strain is experienced by the model with a load at the E2 position. A similar phenomenon can also be observed in Figure 15(b); the model configuration with two stiffeners results in the lowest strain when subjected

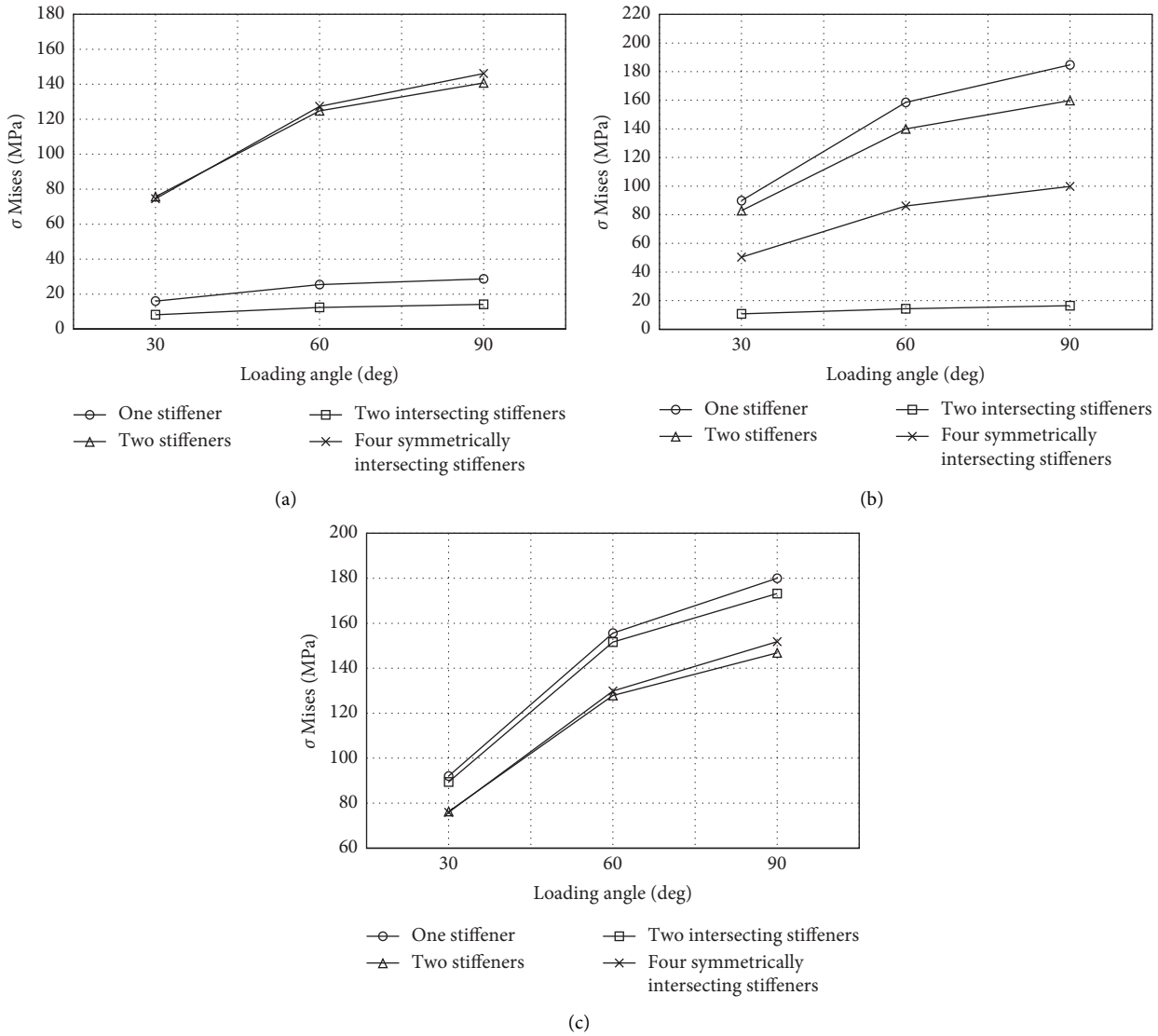

Figure 12: von Mises stress rests at different loading positions. (a) At centered positions. (b) At E2 position. (c) At E3 position.

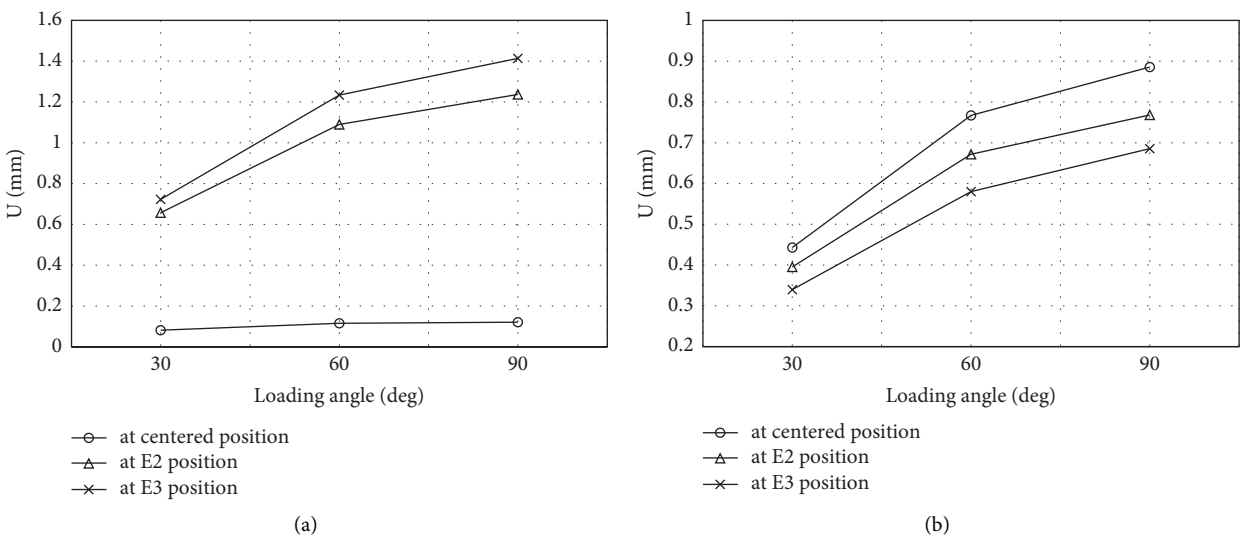

Figure 13: Continued.

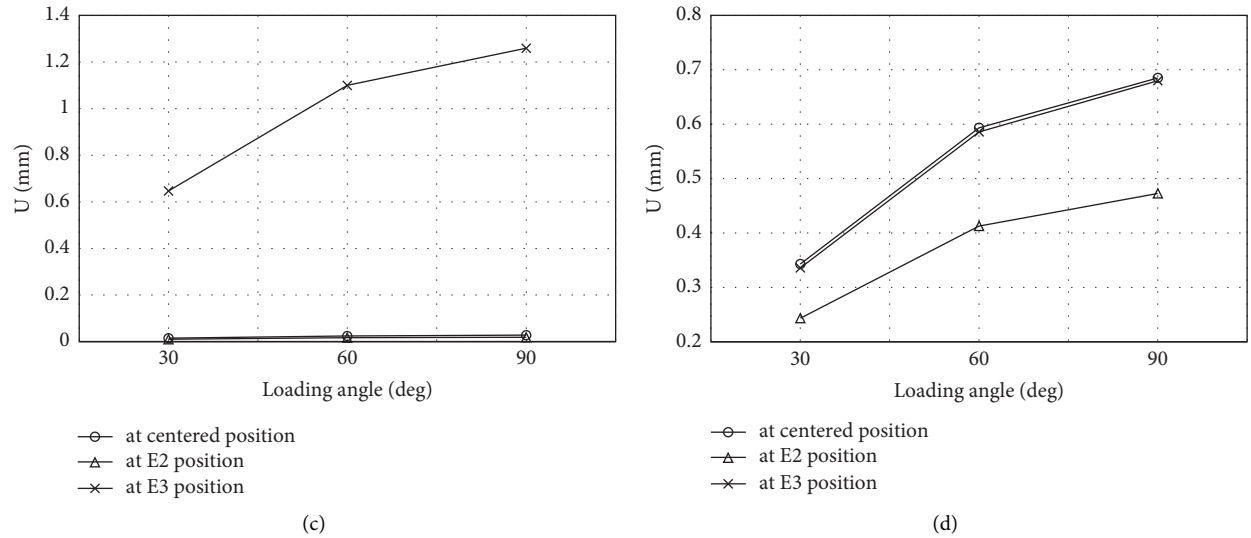

Figure 13: Displacement values for various stiffener configurations. (a) One stiffener. (b) Two stiffeners. (c) Two intersecting stiffeners. (d) Four symmetrically intersecting stiffeners.

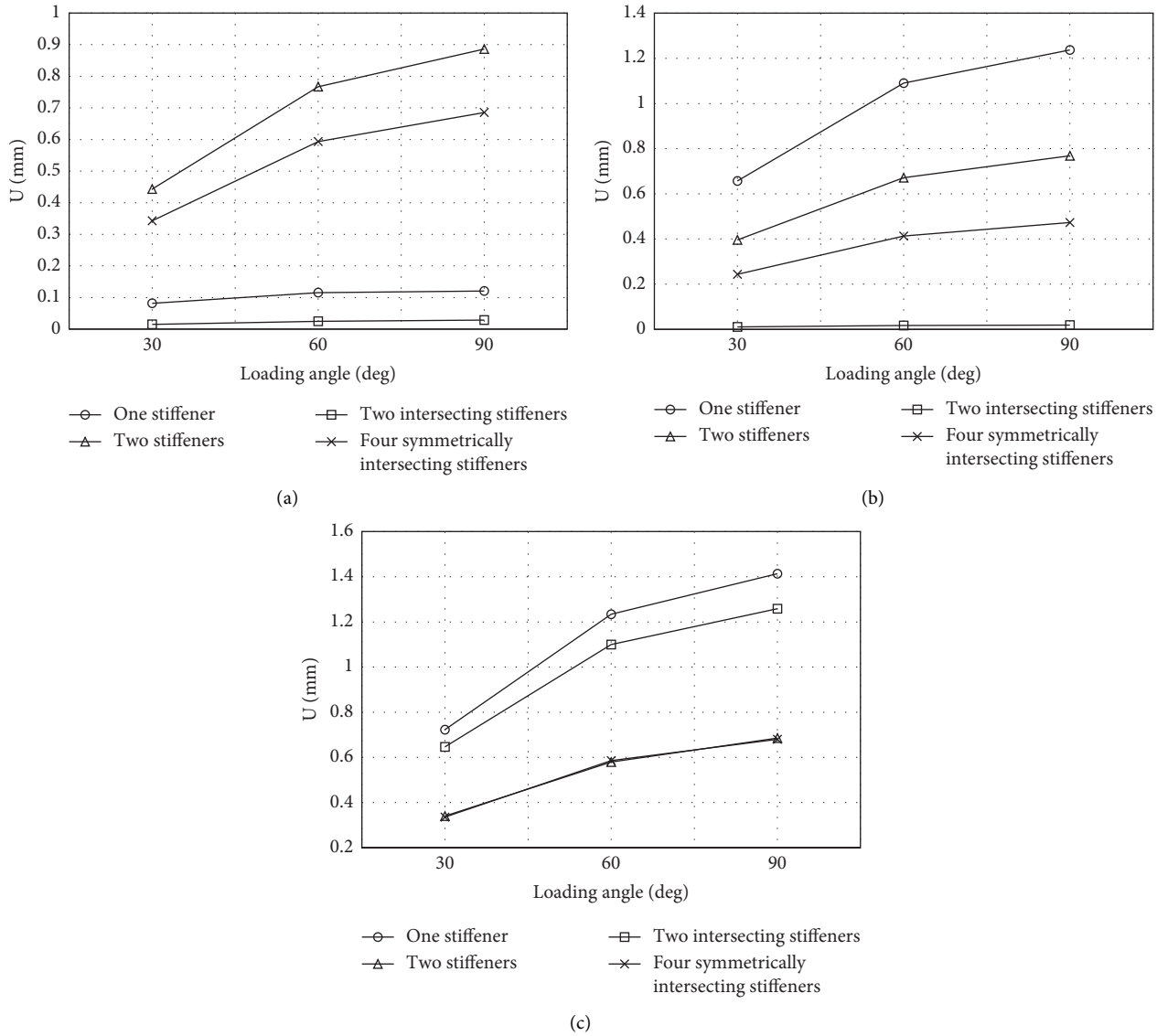

Figure 14: Displacement values at different loading positions. (a) At centered positions. (b) At E2 position. (c) At E3 position.

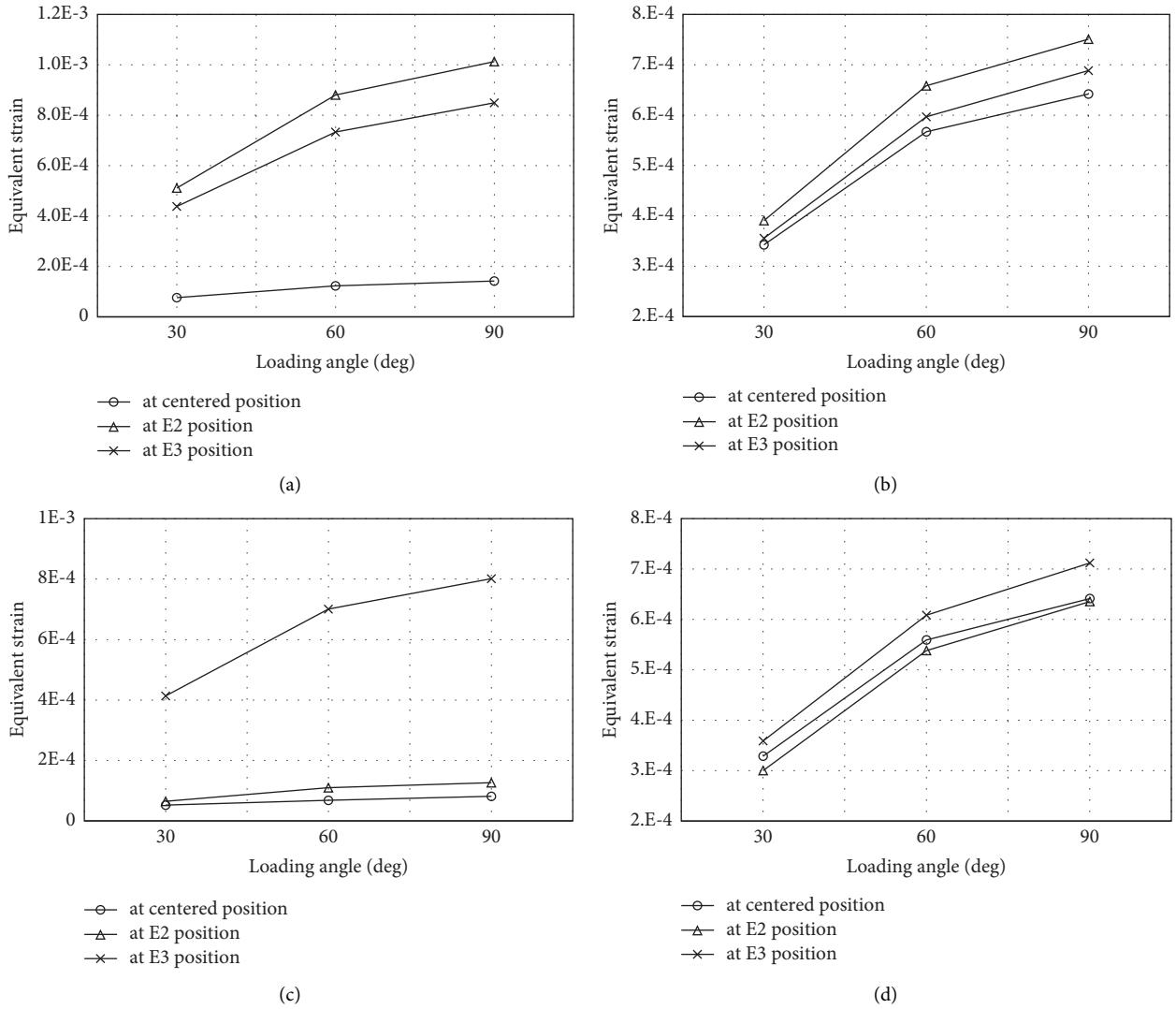

Figure 15: Equivalent strain results for various stiffener configurations. (a) One stiffener. (b) Two stiffeners. (c) Two intersecting stiffeners. (d) Four symmetrically intersecting stiffeners.

to a load at the center of the plate, and the highest value is obtained at the E2 position. Moreover, the strain results in the model with two intersecting stiffeners are shown in Figure 15(c). It can be observed that the model with two intersecting stiffeners is the superior option for withstanding a load applied at the center point of the plate and the E2 position, which have lower strain values. The results indicate that the design is more rigid when subjected to a load that is really in the middle of the stiffener. Furthermore, the equivalent strain in the model with four symmetrically intersecting stiffeners subjected to load at a position near the stiffener is illustrated in Figure 15(d). It can be observed that the strain values of all models are similar. The lowest strain is obtained in the model at the E2 position, and the highest strain is observed in the model with the load at the E3 position.

5.3.2. Comparison of Displacement at Loading Positions for Different Stiffener Configurations. Besides the stress and deformation, the equivalent strain is also essential to determine when selecting the best stiffener model configuration at each load position. The comparison of strain at each load position is depicted in Figure 16. As can be seen, the model with two intersecting stiffeners is the best configuration when it is loaded at the center of the plate, as illustrated in Figure 16(a). A similar result is observed in Figure 16(b), where the model with two intersecting stiffeners is the best configuration when subjected to a load at the E2 position. Further, the best model configurations for the load positioned at E3 are the models with two stiffeners and four symmetrically intersecting stiffeners, which have similar strain values for all loading angles.

5.4. Overall Discussion. The strength assessment of ship plates is required to quantify the deformation and stress states and determine the relationship between the structural responses and designed parameters. The analysis results in Figures 11–16 present the correlation between each structural

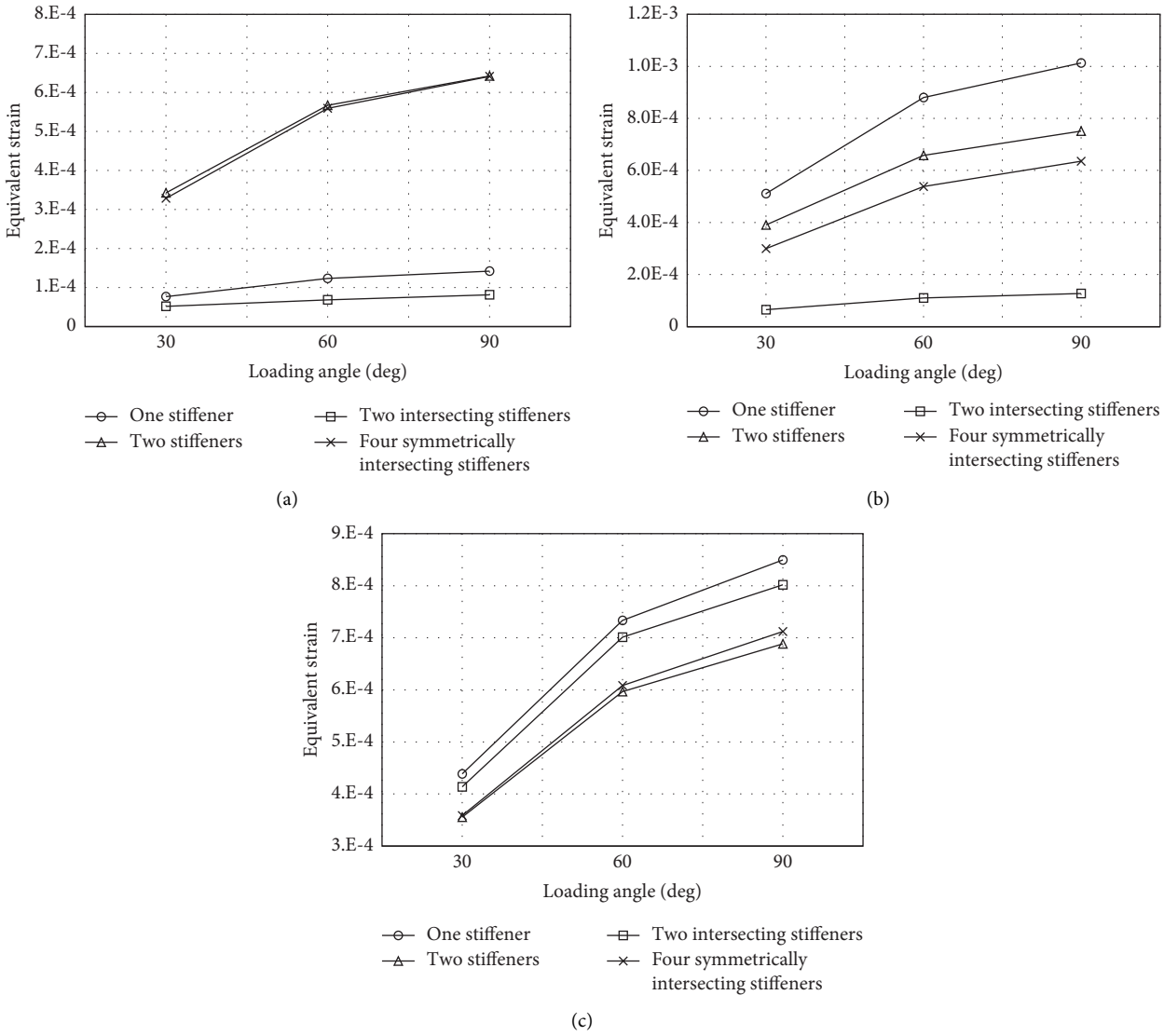

Figure 16: Equivalent strain results for different loading conditions. (a) At centered positions. (b) At E2 position. (c) At E3 position.

behavior and input parameter to determine the function and effectiveness of the stiffener. An overall assessment is needed to quantify the responses and phenomena.

Displacement is used as an indicator to assess the success of the stiffener design configuration. Based on deformation data in Figure 17, model configurations with one stiffener and two intersecting stiffeners are the best designs to withstand a force acting on the center of the plate, and the model with two intersecting stiffeners has the lowest deformation. In this case, the center of the force will be at the center of the stiffener, so with these proposed designs, good results will be obtained with small deformation. This is because these designs are more rigid when subjected to a load in this location. In contrast, the models with two stiffeners and four symmetrically intersecting stiffeners experience higher deformation. The calculation results indicate that deformation is approximately 24 times higher in the model with four symmetrically intersecting stiffeners and up to 31 times higher in the model with two stiffeners.

Further, to conduct deformation assessments in more detail, the influence of the stiffener configuration subjected to loads at random positions (at E2 and E3 positions) was analyzed. Based on the presented data in Figure 17, the model with two intersecting stiffeners is the best option with the lowest deformation when subjected to a load at the E2 position. In contrast, the highest deformation is experienced by the model with one stiffener: the value is about 67 times higher than the deformation in the model with two intersecting stiffeners. This occurs because a large area of the plate is not supported by the stiffener, so more significant deformation occurs. In another loading position (at E3 loading position), the models with two stiffeners and two intersecting stiffeners are the best designs, which experience smaller deformation. On the contrary, the models with one stiffener and two intersecting stiffeners experience twofold higher deformation. These results show that the stiffener is more effective when the force is very close to it. Overall, the models using one stiffener and two intersecting stiffeners are

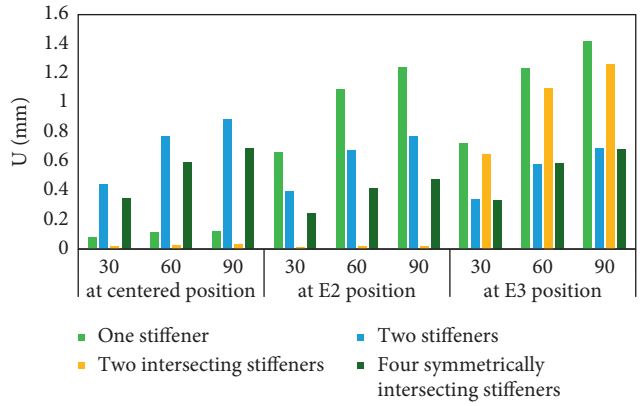

Figure 17: Displacement values in all simulations.

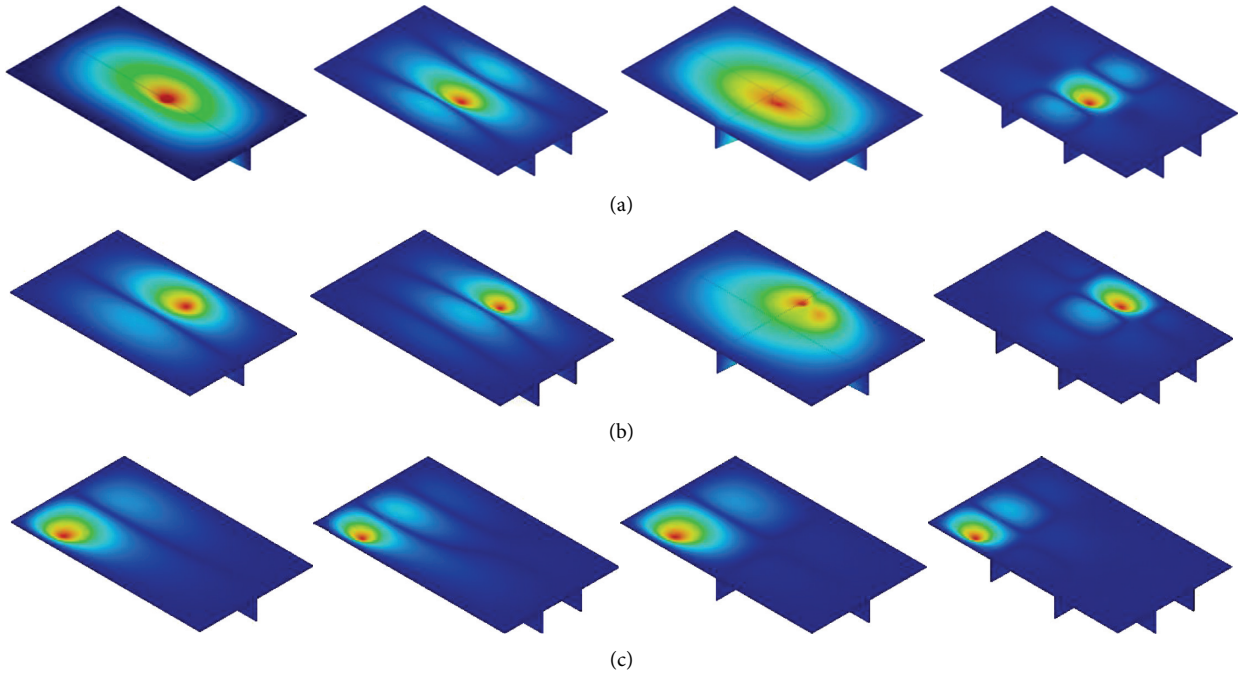

Figure 18: Displacement contours for different loading positions. (a) At center. (b) At E2 load position. (c) At E3 load position.

inferred to be the best alternatives for withstanding a load at the center of the plate. However, the models with two stiffeners and two intersecting stiffeners have a higher level of strength to overcome loads in random positions. The deformation contour at different loading positions at 90 degrees for various models is depicted in Figure 18.

Quantification of the structural results in this work provides a set of reference data that build on pioneering works on plated structures, which predominantly applied shell elements. These works have varied, e.g., nonlinear buckling [47], compressive strength [48, 49], and plate–beam combination [50]. Salomon [51] studied similar subjects to those presented in this work and introduced an analytical theory describing different deflection phenomena on the shell model and 3D model (solid). The findings show that the thickness of the modeled stiffener has a substantial effect on the displacement solution. Future work will expand the current study by conducting the finite element analysis with the same designed configurations, but shell elements will be applied to the geometry. In addition, the stiffener material may be varied as a new variable to verify the theoretical model.

6. Conclusions

This work focuses on the behavior quantification of stiffened plates, which were the subjects of finite element (FE) analysis. Instead of shell elements, this work used solid elements on the plate geometries, and determining the recommended mesh size and configuration was the main goal of this analysis. Based on the convergence assessment, the element length-to-thickness (ELT) ratio for the FE analysis using solid elements is verified to be in the range of 4–10. If a reduction in the processing time is desired, the ratio can be increased to 14, but a proper convergence study is necessary in the first stage. For application to a complex structure, such as a ship hull, increasing the ELT will

certainly be beneficial for reducing the processing time. However, the fidelity of the results also needs to be ensured by applying a convergence test before the main analysis as one of the validation methods.

The results of the meshing criteria were subsequently implemented using the stiffened models, and an integrated analysis was performed to assess the structural loading of the stiffened side hull design, especially when the side hull hits something with a sharp tip. To determine the effectiveness of the stiffener configuration designs, various loading positions and angles were tested to demonstrate the effects of the hull hitting objects from multiple sides. The displacement is used as an indicator of the successful design of the stiffener configuration. From the analysis of the above results, the following conclusions can be drawn:

(1) The stiffened plates with one stiffener and two intersecting stiffeners are suitable for withstanding concentrated loads at the centers of the plates. However, the models with two stiffeners and two intersecting stiffeners have a higher level of strength to overcome loads in random positions.

(2) The number of stiffener configurations influences the effectiveness in reducing the deformation. The results show that when the area of the plate that is not reinforced by the stiffener is smaller, the deformation will be smaller, too. Therefore, higher strength can be obtained with a design, in which the area that is not supported by the stiffener is minimized.

(3) Force at both 30 and 60 degrees leads to the horizontal deformation of the stiffener according to the direction of the force. In contrast, a loading force of 90 degrees causes the stiffened plates to deform vertically according to the force direction. The data show that the greater the angle of the loading direction, the greater the total displacement. This is because when the force has a small angle, part of the force is distributed horizontally.

(4) Based on von Mises stress results, the mechanical properties of medium carbon steel material can withstand 5000 N of the applied load. It can be observed that the obtained stress is smaller than the yield stress. In all model configurations, the proposed design is not damaged after being tested using a load magnitude of 5000 N.

(5) Force that is not perpendicular to the plate (30 and 60 degrees) has a smaller critical strain, lower stress, and less deformation, but it is distributed over a more extensive area.

The current work provides the initial steps to assess meshing criteria for geometries with solid elements, especially plated structures. The latest trends indeed show that the shell entity is more popular as the defined element. Nevertheless, the option to use solid elements is also available, but time and parameter optimizations are required to determine a reasonable configuration when solving physical phenomena using FE calculations. A comparative study to assess shell and solid elements in plated structures is a suitable medium for drawing conclusions regarding the performance of each element, and a continuation of the present work can focus on the analysis of shell elements using the current material, loading, and boundary configurations.

Data Availability

The data supporting the findings of this study are available within the article.

Conflicts of Interest

The authors declare no potential conflicts of interest with respect to the research, authorship, and/or publication of this article.

References

[1] ISSC, "Report of technical committee: ultimate strength III.1," in *Proceedings of the the 19th International Ship and Offshore Structures Congress*, Portugal, Cascais, August 2015.

[2] J. K. Paik, B. J. Kim, and J. K. Seo, "Methods for ultimate limit state assessment of ships and ship-shaped offshore structures: part I-unstiffened plates," *Ocean Engineering*, vol. 35, no. 2, pp. 261–270, 2008.

[3] J. K. Paik, B. J. Kim, and J. K. Seo, "Methods for ultimate limit state assessment of ships and ship-shaped offshore structures: Part II stiffened panels," *Ocean Engineering*, vol. 35, no. 2, pp. 271–280, 2008.

[4] M. C. Xu, D. Yanagihara, M. Fujikubo, and C. Guedes Soares, "Influence of boundary conditions on the collapse behaviour of stiffened panels under combined loads," *Marine Structures*, vol. 34, pp. 205–225, 2013.

[5] N. E. Shanmugam, Z. Dongqi, Y. S. Choo, and M. Arockiaswamy, "Experimental studies on stiffened plates under in-plane load and lateral pressure," *Thin-Walled Structures*, vol. 80, pp. 22–31, 2014.

[6] H. Ma, Q. Xiong, and D. Wang, "Experimental and numerical study on the ultimate strength of stiffened plates subjected to combined biaxial compression and lateral loads," *Ocean Engineering*, vol. 228, p. 108928, 2021.

[7] G.-J. Shi, D.-W. Gao, and H. Zhou, "Analysis of hull girder ultimate strength and residual strength based on IACS CSR-H," *Mathematical Problems in Engineering*, vol. 2019, Article ID 2098492, 11 pages, 2019.

[8] A. R. Prabowo, D. M. Bae, and J. M. Sohn, "Comparing structural casualties of the Ro-Ro vessel using straight and oblique collision incidents on the car deck," *Journal of Marine Science and Engineering*, vol. 7, no. 6, p. 183, 2019.

[9] A. Rio Prabowo, D. Myung Bae, J. Min Sohn, A. Fauzan Zakki, B. Cao, and J. Hyung Cho, "Effects of the rebounding of a striking ship on structural crashworthiness during ship-ship collision," *Thin-Walled Structures*, vol. 115, pp. 225–239, 2017.

[10] M. Zhang, Z. Zhu, Y. Zeng, J. Liu, and Z. Hu, "Analytical method for evaluating the impact response of stiffeners in a ship side shell subjected to bulbous bow collision," *Mathematical Problems in Engineering*, vol. 2020, Article ID 5025438, 11 pages, 2020.

[11] A. R. Prabowo, S. J. Baek, J. H. Byeon, D. M. Bae, J. H. Cho, and J. M. Sohn, "Investigation on the structural damage of a double-hull ship, Part I - ship collision," *Procedia Structural Integrity*, vol. 5, pp. 935–942, 2017.

[12] P. Silveira, A. P. Teixeira, J. R. Figueira, and C. Guedes Soares, "A multicriteria outranking approach for ship collision risk assessment," *Reliability Engineering & System Safety*, vol. 214, Article ID 107789, 2021.

[13] M. A. G. Calle, R. E. Oshiro, and M. Alves, "Ship collision and grounding: scaled experiments and numerical analysis," *International Journal of Impact Engineering*, vol. 103, pp. 195–210, 2017.

[14] A. R. Prabowo, S. I. Cahyono, and J. M. Sohn, "Crashworthiness assessment of thin-walled double bottom tanker: a variety of ship grounding incidents," *Theoretical and Applied Mechanics Letters*, vol. 9, no. 5, pp. 320–327, 2019.

[15] A. R. Prabowo, B. Cao, J. M. Sohn, and D. M. Bae, "Crashworthiness assessment of thin-walled double bottom tanker: influences of seabed to structural damage and damage-energy formulae for grounding damage calculations," *Journal of Ocean Engineering and Science*, vol. 5, no. 4, pp. 387–400, 2020.

[16] A. Negri and P. Marshall, "TBT contamination of remote marine environments: ship groundings and ice-breakers as sources of organotins in the Great Barrier Reef and Antarctica," *Journal of Environmental Management*, vol. 90, no. S1, pp. S31–S40, 2009.

[17] A. R. Prabowo and D. M. Bae, "Environmental risk of maritime territory subjected to accidental phenomena: correlation of oil spill and ship grounding in the Exxon Valdez's case," *Results in Engineering*, vol. 4, Article ID 100035, 2019.

[18] R. E. Gagnon and J. Wang, "Numerical simulations of a tanker collision with a bergy bit incorporating hydrodynamics, a validated ice model and damage to the vessel," *Cold Regions Science and Technology*, vol. 81, pp. 26–35, 2012.

[19] C. Rigueiro, J. Ribeiro, and A. Santiago, "Numerical assessment of the behaviour of a fixed offshore platform subjected to ship collision," *Procedia Engineering*, vol. 199, pp. 2494–2499, 2017.

[20] A. R. Prabowo, F. B. Laksono, and J. M. Sohn, "Investigation of structural performance subjected to impact loading using finite element approach: case of ship-container collision," *Curved and Layered Structures*, vol. 7, no. 1, pp. 17–28, 2020.

[21] A. R. Prabowo, J. H. Byeon, H. J. Cho, J. M. Sohn, D. M. Bae, and J. H. Cho, "Impact phenomena assessment: Part I - structural performance of a tanker subjected to ship grounding at the Arctic," *MATEC Web of Conferences*, vol. 159, p. 02061, 2018.

[22] L. Zhu, W. Liu, H. Fang, J. Chen, Y. Zhuang, and J. Han, "Design and simulation of innovative foam-filled Lattice Composite Bumper System for bridge protection in ship collisions," *Composites Part B: Engineering*, vol. 157, pp. 24–35, 2019.

[23] H. Wael Leheta, S. Farouk Badran, and A. Shawki Elhanafi, "Ship structural integrity using new stiffened plates," *Thin-Walled Structures*, vol. 94, pp. 545–561, 2015.

[24] H. W. Leheta, A. S. Elhanafi, and S. F. Badran, "A numerical study of the ultimate strength of Y-deck panels under longitudinal in-plane compression," *Thin-Walled Structures*, vol. 100, pp. 134–146, 2016.

[25] J. M. Gordo and C. G. Soares, "Compressive tests on short continuous panels," *Marine Structures*, vol. 21, no. 2-3, pp. 113–137, 2008.

[26] J. M. Gordo and C. G. Soares, "Tests on ultimate strength of hull box girders made of high tensile steel," *Marine Structures*, vol. 22, no. 4, pp. 770–790, 2009.

[27] J. M. Gordo and C. Guedes Soares, "Compressive tests on long continuous stiffened panel," *Journal of Offshore Mechanics and Arctic Engineering*, vol. 134, Article ID 021403, 2012.

[28] H. Ren, Y. Liu, C. Li, X. Zhang, and Z. Wu, "Numerical investigation of ultimate strength of stiffened plates with various cross-section forms," in *Proceedings of the 37th International Conference on Ocean, Offshore and Arctic Engineering. OMAE)*, Madrid, Spain, June 2018.

[29] T. Tuswan, K. Abdullah, A. Zubaydi, and A. Budipriyanto, "Finite-element analysis for structural strength assessment of marine sandwich material on ship side-shell structure," *Materials Today: Proceedings*, vol. 13, pp. 109–114, 2019.

[30] A. Tuswan, B. Piscesa, and A. Ismail, "Dynamic characteristic of partially debonded sandwich of ferry ro-ro's car deck: a numerical modeling," *Open Engineering*, vol. 10, no. 1, pp. 424–433, 2020.

[31] T. Tuswan, A. Zubaydi, B. Piscesa et al., "Influence of application of sandwich panel on static and dynamic behaviour of ferry ro-ro ramp door," *Journal of Applied Engineering Science*, vol. 19, no. 1, pp. 208–216, 2021.

[32] S.-E. Kim, G. Papazafeiropoulos, C. Graciano et al., "Optimal design of longitudinal stiffeners of unsymmetric plate girders subjected to pure bending," *Ocean Engineering*, vol. 221, p. 108374, 2021.

[33] D. H. Kim and J. K. Paik, "Ultimate limit state-based multiobjective optimum design technology for hull structural scantlings of merchant cargo ships," *Ocean Engineering*, vol. 129, pp. 318–334, 2017.

[34] C.-Y. Jen and Y.-S. Tai, "Deformation behavior of a stiffened panel subjected to underwater shock loading using the nonlinear finite element method," *Materials & Design*, vol. 31, no. 1, pp. 325–335, 2010.

[35] B. C. Simonsen and P. F. Hansen, "Theoretical and statistical analysis of ship grounding accidents," *Journal of Offshore Mechanics and Arctic Engineering*, vol. 122, no. 3, pp. 200–207, 2000.

[36] A. P. Boresi and R. J. Schmidt, *Advanced Mechanics of Materials*, John Wiley & Sons, Inc., Hoboken, NJ, USA, 6th edition, 2003.

[37] H. S. Alsos and J. Amdahl, "On the resistance to penetration of stiffened plates, Part I - Experiments," *International Journal of Impact Engineering*, vol. 36, no. 6, pp. 799–807, 2009.

[38] St-steel&tube, "Mediium tensile steel—AISI 1045, St-steel&tube: product technical assessment: engineering steel," 2021, https://bit.ly/3wMhOlw.

[39] Interlloy, "1045 medium tensile steel bar, interlloy: enginering steel + alloy," 2021, https://bit.ly/3kpb6PO.

[40] AzoMaterials, "AISI 1045 medium carbon steel, AzoMaterials: editorial feature," 2012, https://bit.ly/3rex7SV.

[41] Fushun Special Steel, "AISI 1045 carbon steel, fushun special steel: alloy structural steel," 2021, https://bit.ly/3B7j4De.

[42] I. Mastrogiannakis and G. C. Vosniakos, "Exploring structural design of the francis hydro-turbine blades using composite materials," *Facta Universitatis – Series: Mechanical Engineering*, vol. 18, no. 1, pp. 43–55, 2020.

[43] R. Törnqvist, *Design of Crashworthy Ship Structure*, Technical University of Denmark, Denmark, Lyngby, 2003.

[44] H. S. Alsos and J. Amdahl, "On the resistance of tanker bottom structures during stranding," *Marine Structures*, vol. 20, no. 4, pp. 218–237, 2007.

[45] A. R. Prabowo, T. Putranto, and J. M. Sohn, "Simulation of the behavior of a ship hull under grounding: effect of applied element size on structural crashworthiness," *Journal of Marine Science and Engineering*, vol. 7, no. 8, p. 270, 2019.

[46] K. J. Bathe, *Finite Element Procedures*, Prentice Hall, Hoboken, NJ, USA, 2014.

[47] E. Gunay, C. Aygun, and Y. O. Yıldız, "Nonlinear buckling finite element analysis of stiffened steel plates," *Advanced Materials Research*, vol. 699, pp. 450–456, 2013.

[48] J. Du, P. Yang, C. Cui, and T. Xia, "Ultimate strength of steel panels and stiffened plates with longitudinal through-thickness cracks under compression," in *Proceedings of the 4th International Conference on Sustainable Energy and Environmental Engineering (ICSEEE 2015)*, pp. 837–843, Shenzhen, China, December 2015.

[49] Y. Cao, R. Zhong, D. Shao, Q. Wang, and X. Guan, "Dynamic analysis of rectangular plate stiffened by any number of beams with different lengths and orientations," *Shock and Vibration*, vol. 2019, Article ID 2364515, 22 pages, 2019.

[50] C. Li, S. Dong, T. Wang, W. Xu, and X. Zhou, "Numerical investigation on ultimate compressive strength of welded stiffened plates built by steel grades of S235-S390," *Applied Sciences*, vol. 9, no. 10, p. 2088, 2019.

[51] A. Salomon, *An Evaluation of Finite Element Models of Stiffened Plates*, Massachusetts Institute of Technology, Cambridge, MA, USA, 2001.